

 Open access • Journal Article • DOI:10.1103/PHYSREVA.64.033812

## **General theory for spontaneous emission in active dielectric microstructures: Example of a fiber amplifier — [Source link](#)**

Thomas Søndergaard, Bjarne Tromborg

**Published on:** 17 Aug 2001 - [Physical Review A](#) (American Physical Society)

**Topics:** [Spontaneous emission](#), [Electromagnetic field](#), [Semiconductor laser theory](#), [Dielectric](#) and [Amplifier](#)

Related papers:

- [Spontaneous emission of a cesium atom near a nanofiber: Efficient coupling of light to guided modes](#)
- [Spontaneous emission rate of an excited atom placed near a nanofiber](#)
- [Optical nanofiber as an efficient tool for manipulating and probing atomic fluorescence](#)
- [Optical Interface Created by Laser-Cooled Atoms Trapped in the Evanescent Field Surrounding an Optical Nanofiber](#)
- [Cavity quantum electrodynamics for a cylinder: Inside a hollow dielectric and near a solid dielectric cylinder](#)

Share this paper:    

View more about this paper here: <https://typeset.io/papers/general-theory-for-spontaneous-emission-in-active-dielectric-39csx8nar2>



**AALBORG UNIVERSITY**  
DENMARK

**Aalborg Universitet**

## **General theory for spontaneous emission in active dielectric microstructures: Example of a fiber amplifier**

Søndergaard, Thomas; Tromborg, Bjarne

*Published in:*  
Physical Review A

*DOI (link to publication from Publisher):*  
[10.1103/PhysRevA.64.033812](https://doi.org/10.1103/PhysRevA.64.033812)

*Publication date:*  
2001

*Document Version*  
Publisher's PDF, also known as Version of record

[Link to publication from Aalborg University](#)

*Citation for published version (APA):*  
Søndergaard, T., & Tromborg, B. (2001). General theory for spontaneous emission in active dielectric microstructures: Example of a fiber amplifier. *Physical Review A*, 64(3), 033812.  
<https://doi.org/10.1103/PhysRevA.64.033812>

### **General rights**

Copyright and moral rights for the publications made accessible in the public portal are retained by the authors and/or other copyright owners and it is a condition of accessing publications that users recognise and abide by the legal requirements associated with these rights.

- Users may download and print one copy of any publication from the public portal for the purpose of private study or research.
- You may not further distribute the material or use it for any profit-making activity or commercial gain
- You may freely distribute the URL identifying the publication in the public portal -

### **Take down policy**

If you believe that this document breaches copyright please contact us at [vbn@aub.aau.dk](mailto:vbn@aub.aau.dk) providing details, and we will remove access to the work immediately and investigate your claim.

# General theory for spontaneous emission in active dielectric microstructures: Example of a fiber amplifier

T. Søndergaard\*

*Research Center COM, Technical University of Denmark, Building 345, DK-2800 Lyngby, Denmark*

B. Tromborg†

*Research Center COM, Technical University of Denmark, Building 345, DK-2800 Lyngby, Denmark*

(Received 30 August 2000; revised manuscript received 20 March 2001; published 17 August 2001)

A model for spontaneous emission in active dielectric microstructures is given in terms of the classical electric field Green's tensor and the quantum-mechanical operators for the generating currents. A formalism is given for calculating the Green's tensor, which does not rely on the existence of a complete power orthogonal set of electromagnetic modes, and the formalism may therefore be applied to microstructures with gain and/or absorption. The Green's tensor is calculated for an optical fiber amplifier, and the spontaneous emission in fiber amplifiers is studied with respect to the position, transition frequency, and vector orientation of a spatially localized current source. Radiation patterns are studied using a Poynting vector approach taking into account amplification or absorption from an active medium in the fiber.

DOI: 10.1103/PhysRevA.64.033812

PACS number(s): 42.50.Ct, 42.55.Wd, 32.70.Cs, 42.81.-i

## I. INTRODUCTION

The spontaneous emission properties of an emitter changes when it is placed in a small cavity [1], between mirrors [2,3], or in a medium with spatially varying dielectric constant [4–8]. The general explanation is that a cavity or a varying dielectric constant will modify the strength and distribution of electromagnetic modes with which an emitter can interact, resulting indirectly in altered spontaneous emission properties. The effect was first noticed by Purcell in 1946 [1] and has since been demonstrated in a number of experiments on Rydberg atoms, quantum dots, and rare-earth materials [9–18]. One of the perspectives of the effect is that spontaneous emission of an emitter can, to some extent, be controlled and even engineered by tailoring the surrounding structure on a transition wavelength scale.

The standard approach to calculation of the rate of spontaneous emission for an atom placed in an empty metallic cavity or in free space, is to expand the radiation field in power orthogonal modes normalized to one quantum of energy and use the Fermi golden rule. If the emitter is embedded in a dielectric material, the coupling between matter and the radiation field requires a QED formulation of Maxwell's equations for the dielectric medium in order to calculate the rate of spontaneous emission from the emitter. For passive media without gain or absorption, it is possible, as in free space, to expand the radiation field in power orthogonal modes and to use the expansion as a basis for quantization. This is, for example, the method for calculating spontaneous emission rates in photonic band-gap structures [19–21], where the local density of electromagnetic modes may be strongly modified and even zero in certain frequency ranges due to a periodically varying dielectric constant [21–23].

If the material is active and has loss and/or gain, the solutions to Maxwell's equations cannot be expanded in power orthogonal modes, and the concept of modes becomes more subtle. In that case, it is convenient to use the electromagnetic fields and generating currents as primary observables represented by operators that are defined by their commutation relations. The relation between field and current operators is given by a classical electric-field Green's tensor. This allows a calculation of spontaneous emission even for extended and dynamically varying structures as, for example, a modulated laser diode. The studies of QED for dielectric materials have essentially followed two parallel approaches in the physics and the quantum electronics communities, respectively. The physics approach [24–37] has focused on the material aspects of QED for dielectrics such as the influence of absorption, dispersion, and inhomogeneities.

The quantum electronics approach (see, for example, the papers [38–49] and references in Ref. [44]), has been driven by studies of spontaneous emission in optical waveguides and has explored the effect of the absence of a complete set of power orthogonal modes. In fact, the phenomenon of excess noise in guided modes introduced by Petermann [38] is, as pointed out first by Haus and Kawakami [39], related to the nonexistence of a complete set of power orthogonal electromagnetic modes. The analyses of spontaneous emission in active dielectric waveguides in Refs. [38–49] are based on the scalar wave equation for the electromagnetic field. The scalar methods give the rate of spontaneous emission into guided modes, but they do not give the total rate of spontaneous emission. This requires taking into account the coupling to the complete radiation field and not only the guided modes.

In this paper we extend the analysis of spontaneous emission, based on the approximate scalar wave equation, to a full vectorial approach valid for general active dielectric microstructures. The total rate of spontaneous emission from an emitter in an active dielectric medium can be expressed in terms of the classical Green's tensor, or to be more precise,

\*FAX: +45 45 93 65 81. Email address: ts@com.dtu.dk

†FAX: +45 45 93 65 81. Email address: bt@com.dtu.dk

the double-transverse part of the tensor. We present a general method for calculating this tensor from complete sets of biorthogonal modes for the vector wave equation. The vectorial nature of the formalism allows calculation of spontaneous emission depending on position, transition frequency, and polarization of the emitter in a dielectric microstructure with loss or gain. Vectorial Green's tensor methods for decay of excited molecules have previously been given for the case of homogeneous absorbing dielectric media [32], for an absorbing dielectric surface [35], and in a series of papers by Tomáš and Lenac for absorbing layered structures [50–52].

We exemplify the method by analyzing spontaneous emission in an optical fiber. The step-index fiber is sufficiently simple to allow analytical solutions for the Green's function for both passive and active fibers; the solutions illustrate some subtle issues related to the singularity of the Green's function that are not easily studied by purely numerical methods. We take into account both position and vector orientation of spatially localized generating currents. Our method allows taking spontaneous emission into account into the radiation modes of the electromagnetic field, and thereby the total rate of spontaneous emission from an emitter embedded in, for example, an active waveguide, may be calculated. Spontaneous emission into radiation modes has previously been considered for passive multilayer dielectric structures [12,53–56], and decay in the presence of passive dielectric cylindrical structures has been investigated in Refs. [57–59]. In the analysis of active fibers, the Green's tensor is calculated exemplifying the general formalism for calculating Green's tensors for the vector case. Another example of calculating Green's tensors for active layered structures is given in Ref. [50].

The paper is organized in the following way. In Sec. II the model for spontaneous emission in active dielectric microstructures is given. The general principle for obtaining the electric-field Green's tensor is given in Sec. III. Using this principle the transverse electric-field Green's tensor is derived for the case of active optical fibers in Sec. IV. Position dependence and transition-frequency dependence of spontaneous emission for the passive fiber is given in Sec. V. Radiation patterns obtained using a Poynting vector approach for the active fiber are presented in Sec. VI. Our conclusion is given in Sec. VII.

## II. MODEL FOR SPONTANEOUS EMISSION

In this section we present a general Green's tensor model for calculating the rate of spontaneous emission in a material with a position dependent dielectric constant  $\varepsilon(\mathbf{r})$ . The model allows  $\varepsilon$  to be complex and thus to represent materials with absorption or gain. For simplicity, we treat  $\varepsilon(\mathbf{r})$  as a scalar. There is no problem in principle to let  $\varepsilon(\mathbf{r})$  represent a tensor, and thus to include the case of birefringent materials, but the notation will of course be less transparent. Our model does require a complete set of biorthogonal modes.

The spontaneous emission in the material may be considered as being generated by a distribution of spontaneous currents. The positive frequency part of the current density is represented by an operator  $\hat{\mathbf{j}}(\mathbf{r}, t)$  in the Heisenberg picture.

The real current density is therefore  $\hat{\mathbf{j}} + \hat{\mathbf{j}}^\dagger$ , where  $(\dagger)$  denotes Hermitian conjugation, and where

$$\hat{\mathbf{j}}(\mathbf{r}, t) = \frac{1}{2\pi} \int_0^\infty \hat{\mathbf{j}}(\mathbf{r}; \omega) e^{-i\omega t} d\omega, \quad (1)$$

the integration being only over positive angular frequencies  $\omega$ .

The current density is the sum of two parts  $\hat{\mathbf{j}}_T(\mathbf{r}, t)$  and  $\hat{\mathbf{j}}_{GL}(\mathbf{r}, t)$  with  $\nabla \cdot \hat{\mathbf{j}}_T = 0$  and  $\nabla \times (\hat{\mathbf{j}}_{GL}/\varepsilon) = \mathbf{0}$  [60]. It is actually only the transverse part of the currents  $\hat{\mathbf{j}}_T(\mathbf{r}, t)$ , which contributes to spontaneous emission; the part  $\hat{\mathbf{j}}_{GL}(\mathbf{r}, t)$  contributes to the nonradiative decay rate [32]. For a homogeneous medium with constant  $\varepsilon$ , the component  $\hat{\mathbf{j}}_{GL}$  is simply the longitudinal part, but for nonhomogeneous media,  $\hat{\mathbf{j}}_{GL}$  is the generalized longitudinal part. Notice, that in splitting the current into  $\hat{\mathbf{j}}_T$  and  $\hat{\mathbf{j}}_{GL}$  the transverse part is also affected by  $\varepsilon$ , when this is nonuniform.

The average rate of energy dissipation, due to spontaneous emission, is given in terms of the currents  $\hat{\mathbf{j}}_T$  by

$$\langle P \rangle = - \int \langle \hat{\mathbf{j}}_T^\dagger(\mathbf{r}, t) \cdot \hat{\mathbf{E}}(\mathbf{r}, t) + \hat{\mathbf{E}}^\dagger(\mathbf{r}, t) \cdot \hat{\mathbf{j}}_T(\mathbf{r}, t) \rangle d^3r, \quad (2)$$

where the angled brackets  $\langle \dots \rangle$  denote ensemble and time averaging, and  $\hat{\mathbf{E}}(\mathbf{r}, t)$  is the positive frequency part of the electric-field operator. The field is itself generated by the transverse currents and satisfies the inhomogeneous wave equation

$$[-\nabla \times \nabla \times + k_0^2 \varepsilon(\mathbf{r})] \hat{\mathbf{E}}(\mathbf{r}; \omega) = -i\omega \mu_0 \hat{\mathbf{j}}_T(\mathbf{r}; \omega) \quad (3)$$

in the frequency domain. Here  $k_0 = \omega/c$  is the wave number,  $c$  is the speed of light, and  $\mu_0$  is the permeability, all for vacuum. The solution to Eq. (3) may be written as

$$\hat{\mathbf{E}}(\mathbf{r}; \omega) = -i\omega \mu_0 \int \mathbf{G}(\mathbf{r}, \mathbf{r}'; \omega) \cdot \hat{\mathbf{j}}_T(\mathbf{r}'; \omega) d^3r' \quad (4)$$

in terms of the classical Green's tensor  $\mathbf{G}(\mathbf{r}, \mathbf{r}'; \omega)$ . It is defined as a solution to the equation

$$[-\nabla \times \nabla \times + k_0^2 \varepsilon(\mathbf{r})] \mathbf{G}(\mathbf{r}, \mathbf{r}'; \omega) = \mathbf{I} \delta(\mathbf{r} - \mathbf{r}'), \quad (5)$$

where  $\delta$  is the Dirac delta function, and  $\mathbf{I}$  is the unit  $3 \times 3$  tensor. We shall only deal with the retarded Green's tensor,  $\lim_{\epsilon \rightarrow 0^+} \mathbf{G}(\mathbf{r}, \mathbf{r}'; \omega + i\epsilon)$ , which ensures a causal relationship between  $\hat{\mathbf{E}}(\mathbf{r}, t)$  and  $\hat{\mathbf{j}}_T(\mathbf{r}, t)$ .

Insertion of Eq. (4) in Eq. (2) leads to

$$\begin{aligned} \langle P \rangle = & - \frac{i\mu_0}{(2\pi)^2} \int \langle \hat{\mathbf{j}}_T^\dagger(\mathbf{r}; \omega) \cdot \{ \omega' \mathbf{G}(\mathbf{r}, \mathbf{r}'; \omega') \\ & - \omega \mathbf{G}^\dagger(\mathbf{r}', \mathbf{r}; \omega) \} \cdot \hat{\mathbf{j}}_T(\mathbf{r}'; \omega') \rangle d^3r d^3r' d\omega d\omega'. \end{aligned} \quad (6)$$

It is often convenient to drop the restriction that the currents have to be transverse by instead using the double-transverse Green's tensor  $\mathbf{G}_T$  defined by

$$\mathbf{G}_T(\mathbf{r}, \mathbf{r}'; \omega) = \int \delta_T^\dagger(\mathbf{r}, \mathbf{r}_1) \cdot \mathbf{G}(\mathbf{r}_1, \mathbf{r}_2; \omega) \cdot \delta_T(\mathbf{r}_2, \mathbf{r}') d^3 r_1 d^3 r_2. \quad (7)$$

The transverse delta function  $\delta_T(\mathbf{r}, \mathbf{r}')$  is the operator that projects an arbitrary vector function into its transverse part [26,61]. The construction of  $\delta_T$  is presented in Appendix B.

The spontaneous currents are assumed to be  $\delta$  correlated in space and frequency, i.e.,

$$\langle \hat{j}_l^\dagger(\mathbf{r}; \omega) \hat{j}_m(\mathbf{r}'; \omega') \rangle = 2D_{ml}(\mathbf{r}; \omega) \delta(\mathbf{r} - \mathbf{r}') 2\pi \delta(\omega - \omega'), \quad (8)$$

where  $\hat{j}_l$  is the  $l$ th component of the current density  $\hat{\mathbf{j}}$ , and  $D_{ml}$  is the element  $ml$  of the diffusion tensor  $\mathbf{D}$ . The optical transitions that contribute to the spontaneous emission, and therefore to the diffusion tensor, will also give a contribution  $\epsilon_{sp}$  to the dielectric tensor. The two tensors are related by the fluctuation-dissipation theorem [44]

$$\mathbf{D} = \hbar \omega^2 \epsilon_0 n_{sp} \text{Im}(\epsilon_{sp}), \quad (9)$$

i.e., the diffusion tensor is proportional to the imaginary part of  $\epsilon_{sp}$ . The factor  $n_{sp}$  is the population inversion factor for the involved quantum states, and  $\epsilon_0$  is the vacuum permittivity.

The rate of spontaneous emission  $\Gamma$ , i.e., the number of spontaneously emitted photons per unit time, can now be obtained from the rate of energy dissipation by introducing Eq. (8) in Eq. (6) and dividing the integrand by the photon energy  $\hbar \omega$ . This results in the following simple expression for  $\Gamma$ :

$$\Gamma = - \frac{2\mu_0}{\hbar 2\pi} \text{Im} \left( \int \text{Tr} \{ 2\mathbf{D}(\mathbf{r}; \omega) \cdot \mathbf{G}_T(\mathbf{r}, \mathbf{r}; \omega) \} d^3 r d\omega \right), \quad (10)$$

where ‘‘Tr’’ indicates the trace of the matrix product. We will focus on the case where a dipole emitter is localized at  $\mathbf{r}_0$ , and the transition frequency is  $\omega_0$ . The diffusion tensor is then given by

$$2\mathbf{D} = \omega_0^2 \boldsymbol{\mu} \boldsymbol{\mu}^\dagger \delta(\mathbf{r} - \mathbf{r}_0) 2\pi \delta(\omega - \omega_0), \quad (11)$$

where  $\boldsymbol{\mu}$  is the dipole vector, and the rate of spontaneous emission becomes [32]

$$\Gamma = - \frac{2\mu_0 \omega_0^2}{\hbar} \text{Im} [ \boldsymbol{\mu}^\dagger \cdot \mathbf{G}_T(\mathbf{r}_0, \mathbf{r}_0; \omega_0) \cdot \boldsymbol{\mu} ]. \quad (12)$$

The expression (12) allows us to calculate the rate of spontaneous emission from dipoles, even if the dielectric material is a gain medium at the transition frequency  $\omega_0$ . In that case, the radiation observed outside the material consists of amplified spontaneous emission from the dipole as well as amplified spontaneous emission from the gain medium, and the spontaneous emission rate  $\Gamma$  cannot be determined by simply

counting the emitted photons. However, if the dipole radiation is due to different processes than the processes that provide the gain, it may nevertheless be possible to verify the expression (12) experimentally. In the following, we present a theoretical method for calculating  $\Gamma$ , and we demonstrate the method for the example of an optical fiber.

### III. CONSTRUCTION OF THE ELECTRIC-FIELD TRANSVERSE GREEN'S TENSOR

This section concerns the general principles for construction of the electric-field Green's tensor  $\mathbf{G}(\mathbf{r}, \mathbf{r}'; \omega)$  defined by Eq. (5). Instead of dealing with the wave equation in the form (3), it is convenient to introduce the vector function [26]

$$\mathbf{g}(\mathbf{r}) = \sqrt{\epsilon(\mathbf{r})} \mathbf{E}(\mathbf{r}), \quad (13)$$

and to rewrite the wave equation (3) in terms of  $\mathbf{g}(\mathbf{r})$ :

$$- \frac{1}{\sqrt{\epsilon(\mathbf{r})}} \nabla \times \nabla \times \frac{\mathbf{g}(\mathbf{r})}{\sqrt{\epsilon(\mathbf{r})}} + k_0^2 \mathbf{g}(\mathbf{r}) = -i\omega\mu_0 \frac{\mathbf{j}_T(\mathbf{r})}{\sqrt{\epsilon(\mathbf{r})}}. \quad (14)$$

The argument  $\omega$  has been suppressed for simplicity. We will first derive the Green's tensor  $\mathbf{G}_g(\mathbf{r}, \mathbf{r}')$  for  $\mathbf{g}(\mathbf{r})$ ; by Eq. (13) the Green's tensor  $\mathbf{G}(\mathbf{r}, \mathbf{r}')$  for the electric field is then obtained from the relation

$$\mathbf{G}_g(\mathbf{r}, \mathbf{r}') = \sqrt{\epsilon(\mathbf{r})} \mathbf{G}(\mathbf{r}, \mathbf{r}') \sqrt{\epsilon(\mathbf{r}')}. \quad (15)$$

We define an operator  $\mathcal{H}$  acting on  $\mathbf{g}(\mathbf{r})$  by writing the left-hand side of Eq. (14) as  $\mathcal{H}\mathbf{g}$ . The equation for the Green's tensor  $\mathbf{G}_g(\mathbf{r}, \mathbf{r}')$  may then be written as

$$\mathcal{H}\mathbf{G}_g(\mathbf{r}, \mathbf{r}') = \mathbf{I} \delta(\mathbf{r} - \mathbf{r}'). \quad (16)$$

The operator  $\mathcal{H}$  was introduced by Glauber and Lewenstein in their theory of quantum electrodynamics of dielectric media [26]. For passive dielectric media with real  $\epsilon(\mathbf{r})$ , the operator is Hermitian, but it is non-Hermitian if  $\epsilon(\mathbf{r})$  is complex. The Hermitian conjugate  $\mathcal{H}^\dagger$  is obtained from  $\mathcal{H}$  by replacing  $\epsilon(\mathbf{r})$  by its complex conjugate. In both cases we can assume, that for each set  $(\mathbf{g}_n, \lambda_n)$  of eigensolutions to  $\mathcal{H}\mathbf{g}_n = \lambda_n \mathbf{g}_n$ , there exists a set of eigensolutions  $(\tilde{\mathbf{g}}_n, \lambda_n^*)$  to  $\mathcal{H}^\dagger \tilde{\mathbf{g}}_n = \lambda_n^* \tilde{\mathbf{g}}_n$ , such that the biorthogonality condition

$$\int [\tilde{\mathbf{g}}_n(\mathbf{r})]^* \cdot \mathbf{g}_m(\mathbf{r}) d^3 r = N_n \delta_{nm} \quad (17)$$

and the completeness relation

$$\sum_n \frac{\mathbf{g}_n(\mathbf{r}) \tilde{\mathbf{g}}_n^*(\mathbf{r}')}{N_n} = \mathbf{I} \delta(\mathbf{r} - \mathbf{r}') \quad (18)$$

are satisfied. Here, the asterisk (\*) denotes complex conjugation. The eigenfunction  $\tilde{\mathbf{g}}_n(\mathbf{r})$  is denoted the adjoint of  $\mathbf{g}_n(\mathbf{r})$ . The eigensolutions  $\mathbf{g}_n$  are degenerate, so the assignment of the adjoint solution is not unique, but it can be chosen such that Eqs. (17) and (18) are fulfilled. The actual choice may

be adapted to the specific structure under consideration, as we will demonstrate for the example of an optical fiber. The summation sign in Eq. (18) represents an integration for the case of a continuum of eigensolutions and a summation for discrete eigensolutions. Similarly, the symbol  $\delta_{nm}$  in Eq. (17) represents a Dirac delta function for eigensolutions in the continuous spectrum of eigenvalues, and a Kronecker delta function for discrete eigensolutions.

By the completeness relation (18), the Green's tensor  $\mathbf{G}_g(\mathbf{r}, \mathbf{r}')$  becomes

$$\mathbf{G}_g(\mathbf{r}, \mathbf{r}') = \sum_n \frac{\mathbf{g}_n(\mathbf{r}) \tilde{\mathbf{g}}_n^*(\mathbf{r}')}{N_n \lambda_n}, \quad (19)$$

as can be seen by inserting Eq. (19) in Eq. (16). Equation (15) finally leads to the expression

$$\mathbf{G}(\mathbf{r}, \mathbf{r}'; \omega) = \sum_n \frac{\mathbf{E}_n(\mathbf{r}) [\tilde{\mathbf{E}}_n(\mathbf{r}')]^*}{N_n \lambda_n} \quad (20)$$

for the Green's tensor for the electric field. The electric field  $\mathbf{E}_n = \mathbf{g}_n / \sqrt{\varepsilon}$  is a solution to

$$-\nabla \times \nabla \times \mathbf{E}_n + k_0^2 \varepsilon(\mathbf{r}) \mathbf{E}_n = \lambda_n \varepsilon(\mathbf{r}) \mathbf{E}_n, \quad (21)$$

and  $\tilde{\mathbf{E}}_n = \tilde{\mathbf{g}}_n / \sqrt{\varepsilon^*}$ . The normalization factor  $N_n$  is

$$N_n = \int [\tilde{\mathbf{g}}_n(\mathbf{r})]^* \cdot \mathbf{g}_n(\mathbf{r}) d^3 r = \int \varepsilon(\mathbf{r}) [\tilde{\mathbf{E}}_n(\mathbf{r})]^* \cdot \mathbf{E}_n(\mathbf{r}) d^3 r. \quad (22)$$

The solutions to Eq. (21) must satisfy the equation

$$k_0^2 \nabla \cdot [\varepsilon(\mathbf{r}) \mathbf{E}_n(\mathbf{r})] = \lambda_n \nabla \cdot [\varepsilon(\mathbf{r}) \mathbf{E}_n(\mathbf{r})], \quad (23)$$

so we have either

$$\nabla \cdot [\varepsilon(\mathbf{r}) \mathbf{E}_n(\mathbf{r})] = 0, \quad (24)$$

which describes field solutions in the absence of electric charges, or else  $\nabla \cdot [\varepsilon(\mathbf{r}) \mathbf{E}_n(\mathbf{r})] \neq 0$ , and hence  $\lambda_n = k_0^2$ . In the latter case, the eigenvalue problem reduces to

$$\nabla \times \nabla \times \mathbf{E}_n(\mathbf{r}) = \mathbf{0}, \quad (25)$$

which has solutions of the form

$$\mathbf{E}_n(\mathbf{r}) = \nabla \phi_n(\mathbf{r}), \quad (26)$$

where  $\phi_n(\mathbf{r})$  are scalar functions. They have to fulfill the biorthogonality condition

$$\int \varepsilon(\mathbf{r}) \nabla \phi_n(\mathbf{r}) \cdot \nabla [\tilde{\phi}_m(\mathbf{r})]^* d^3 r = M_n \delta_{nm}, \quad (27)$$

and this can be achieved by choosing  $[\phi_n(\mathbf{r}), \sigma_n]$  to be a complete set of solutions to the eigenvalue problem for the scalar wave equation

$$\nabla \cdot [\varepsilon(\mathbf{r}) \nabla \phi_n] = \sigma_n \phi_n. \quad (28)$$

The set  $[\tilde{\phi}_n(\mathbf{r}), \sigma_n^*]$  is the corresponding set of adjoint solutions. It follows from Eq. (27) and Eq. (28) that the normalization factor  $M_n$  is given by

$$M_n = -\sigma_n \int [\tilde{\phi}_n(\mathbf{r})]^* \phi_n(\mathbf{r}) d^3 r. \quad (29)$$

These considerations lead to a Green's tensor  $\mathbf{G}(\mathbf{r}, \mathbf{r}'; \omega)$ , which is the sum of two terms

$$\mathbf{G} = \mathbf{G}_{GT} + \mathbf{G}_L, \quad (30)$$

where  $\mathbf{G}_{GT}$  is the sum (20) over solutions to Eq. (21) and Eq. (24). It is therefore generalized transverse, i.e.,  $\nabla \cdot (\varepsilon \mathbf{G}_{GT}) = 0$ . The other part  $\mathbf{G}_L$  contains only longitudinal eigenfunctions, i.e.,

$$\mathbf{G}_L(\mathbf{r}, \mathbf{r}'; \omega) = \sum_n \frac{\nabla \phi_n(\mathbf{r}) [\nabla \tilde{\phi}_n(\mathbf{r}')]^*}{M_n k_0^2}. \quad (31)$$

Here we note that the field obtained by inserting the Green's tensor (30) and any current density into Eq. (4) can always be split into a generalized transverse part and a purely longitudinal part. It is then seen using these fields and current densities in Eq. (3) that the current density must consist of a purely transverse part  $\mathbf{j}_T$  with  $\nabla \cdot \mathbf{j}_T = 0$  generating the generalized transverse field, and a part  $\mathbf{j}_{GL}$  with  $\nabla \times (\mathbf{j}_{GL} / \varepsilon) = \mathbf{0}$  generating the longitudinal field. We also note, that by choosing  $(\phi_n, \sigma_n)$  to be a complete set of eigensolutions to Eq. (28), we ensure by construction that a current  $\mathbf{j}$  with a longitudinal component in Eq. (4) will generate an electric field that satisfies the Coulomb equation  $\nabla \cdot (\varepsilon \mathbf{E}) = -i \nabla \cdot \mathbf{j} / (\omega \varepsilon_0)$ .

We shall only be concerned with the double-transverse Green's tensor Eq. (7). Inserting Eq. (30) in Eq. (7) gives

$$\mathbf{G}_T(\mathbf{r}, \mathbf{r}'; \omega) = \sum_n \frac{\mathbf{E}_n^T(\mathbf{r}) [\tilde{\mathbf{E}}_n^T(\mathbf{r}')]^*}{\lambda_n \int \varepsilon(\mathbf{r}) [\tilde{\mathbf{E}}_n(\mathbf{r})]^* \cdot \mathbf{E}_n(\mathbf{r}) d^3 r} + \delta_T^\dagger \mathbf{G}_L \delta_T, \quad (32)$$

where

$$\mathbf{E}_n^T(\mathbf{r}) = \int \delta_T^\dagger(\mathbf{r}, \mathbf{r}') \cdot \mathbf{E}_n(\mathbf{r}') d^3 r', \quad (33)$$

and  $\mathbf{E}_n$  are the generalized transverse solutions to Eq. (21) and Eq. (24). The transverse delta operator  $\delta_T$  is given in Appendix B. For real  $\varepsilon$ , we have  $\mathbf{E}_n^T = \mathbf{E}_n$ ,  $\delta_T^\dagger \mathbf{G}_L \delta_T = \mathbf{0}$  and hence  $\mathbf{G}_T = \mathbf{G}_{GT}$ , but this does not hold for complex  $\varepsilon$ . In the next section this general approach to the electric-field double-transverse Green's tensor is applied to the case of active optical fibers.

#### IV. TRANSVERSE GREEN'S TENSOR FOR THE ACTIVE OPTICAL FIBER

In this section the general principles for the construction of the electric-field Green's tensor, given in the previous section, is applied to the case of an active optical fiber. The

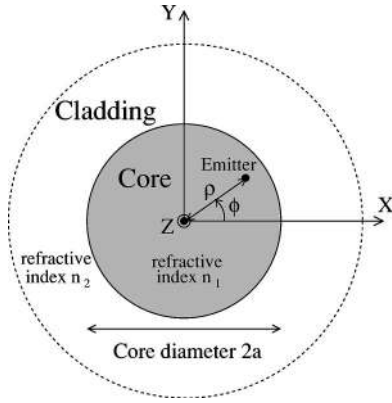


FIG. 1. Illustration of the circular step-index optical fiber with core refractive index  $n_1$ , cladding refractive index  $n_2$ , and core diameter  $2a$ . A Cartesian coordinate system  $(x, y, z)$  is introduced with the origin placed in the center of the fiber core, and with the fiber oriented along the  $z$  axis. The position of a point source is given by  $(\rho, \phi, z)$ .

details of the calculation is given in the Appendices.

A schematic of the circular step-index optical fiber is shown in Fig. 1. The structure consists of a circular core region with refractive index  $n_1$  surrounded by a cladding region with refractive index  $n_2$ . The diameter of the core is denoted  $2a$ . The extent of the cladding region is assumed to be infinite. A Cartesian coordinate system  $(x, y, z)$  is introduced with the origin in the center of the fiber core. The fiber is oriented along the  $z$  axis, and the position of a point source is given in cylindrical coordinates by  $(\rho, \phi, z)$ . The spontaneous emission depends on both the position and the orientation of the dipole vector  $\boldsymbol{\mu}$ . In this paper we will consider spontaneous emission for emitters oriented along the  $z$  axis, and for emitters oriented in the  $xy$  plane. In the latter case, we will be interested only in the average emission for dipole vectors oriented along the two in-plane directions  $x$  and  $y$ . The total spontaneous emission for these two types of orientation of the generating currents depends only on the radius  $\rho$  due to symmetry considerations.

The formalism developed in Sec. III for calculating the transverse electric-field Green's tensor requires that the generalized transverse eigensolutions  $[\lambda_n; \mathbf{E}_n(\mathbf{r})]$  of Eq. (21) are obtained.

Taking advantage of the circular symmetry of the problem we will quantize the eigenfunctions  $\mathbf{E}_n(\mathbf{r})$  in cylindrical wave functions. Generalized transverse solutions may be constructed by introducing both the electric field  $\mathbf{E}_n$  and the magnetic field  $\mathbf{H}_n$  given by  $\mathbf{H}_n = \nabla \times \mathbf{E}_n / (i\tilde{\omega}_n \mu_0)$ , where  $\tilde{\omega}_n^2 = \omega^2 - \lambda_n c^2$ , and requiring the tangential components of both fields to be constant across the interface between core and cladding.

The eigenmodes  $\mathbf{E}_n$  and the corresponding fields  $\mathbf{H}_n$  may be quantized in cylindrical wave functions in the form

$$\mathbf{E}_\alpha(\rho, \phi, z) = \mathbf{F}_\alpha(\rho) e^{im\phi} e^{i\beta z}, \quad (34)$$

$$\mathbf{H}_\alpha(\rho, \phi, z) = \mathbf{G}_\alpha(\rho) e^{im\phi} e^{i\beta z}, \quad (35)$$

where  $\alpha$  represents the quantization indices. In a cylindrical coordinate system the vectors  $\mathbf{F}_\alpha(\rho)$  and  $\mathbf{G}_\alpha(\rho)$  do not depend on the angle  $\phi$ , and therefore the  $\phi$  dependence of these vectors has been suppressed. The eigensolutions may be divided into two types of solutions, which we refer to as radiation modes and guided modes, respectively. For radiation modes, there are four quantization indices  $\alpha = \{m, p, \beta, q\}$ , where  $\beta$  is the component of the wave vector along the  $z$  axis,  $q$  represents the magnitude of the wave vector perpendicular to the  $z$  axis,  $m$  is the angular momentum, and the index  $p$  is used to distinguish between two degenerate polarization modes for given  $m, \beta$ , and  $q$ .

In the first part of this section, we will consider the contribution to the Green's tensor related to radiation modes, and then come back to the contribution related to guided modes at the end of the section.

The substitution of Eq. (34) into the eigenvalue problem (21), leads to the following differential equations for the  $z$  component of the electric field for the optical fiber

$$\begin{aligned} (\kappa\rho)^2 \frac{\partial^2 F_{z,\alpha}}{\partial(\kappa\rho)^2} + \kappa\rho \frac{\partial F_{z,\alpha}}{\partial(\kappa\rho)} + [(\kappa\rho)^2 - m^2] F_{z,\alpha} &= 0, \quad \rho \leq a, \\ (q\rho)^2 \frac{\partial^2 F_{z,\alpha}}{\partial(q\rho)^2} + q\rho \frac{\partial F_{z,\alpha}}{\partial(q\rho)} + [(q\rho)^2 - m^2] F_{z,\alpha} &= 0, \quad \rho > a, \end{aligned} \quad (36)$$

where

$$\begin{aligned} \kappa^2 &= (k_0^2 - \lambda_\alpha) \varepsilon_1 - \beta^2, \\ q^2 &= (k_0^2 - \lambda_\alpha) \varepsilon_2 - \beta^2. \end{aligned} \quad (37)$$

Here  $\lambda_\alpha$  is the eigenvalue of the eigensolution with quantization indices  $\alpha$ , and  $\varepsilon_1 = n_1^2$  and  $\varepsilon_2 = n_2^2$  represent the dielectric constant in the core and cladding of the fiber, respectively.

For radiation modes, eigensolutions exist for all combinations of  $m, \beta$ , and  $q$ . By applying the boundary condition that the field amplitude must remain finite, both in the core and cladding, the  $z$  component of the two fields  $\mathbf{F}_\alpha$  and  $\mathbf{G}_\alpha$  may be written in the form

$$F_{z,\alpha}(\rho) = \begin{cases} A_\alpha J_m(\kappa\rho), & \rho \leq a \\ C_\alpha^+ H_m^{(1)}(q\rho) + C_\alpha^- H_m^{(2)}(q\rho), & \rho > a \end{cases} \quad (38)$$

$$G_{z,\alpha}(\rho) = \begin{cases} B_\alpha J_m(\kappa\rho), & \rho \leq a \\ D_\alpha^+ H_m^{(1)}(q\rho) + D_\alpha^- H_m^{(2)}(q\rho), & \rho > a. \end{cases} \quad (39)$$

The other components  $F_{\rho,\alpha}$ ,  $F_{\phi,\alpha}$ ,  $G_{\rho,\alpha}$ , and  $G_{\phi,\alpha}$  may be expressed in terms of  $F_{z,\alpha}$  and  $G_{z,\alpha}$  by using Maxwell's equations [62].

In the above equations,  $J_m$  is the Bessel function of the first kind of order  $m$ , and  $H_m^{(1)}$ ,  $H_m^{(2)}$  are the Hankel functions of the first and second kind of order  $m$ . The boundary conditions, which require  $F_{z,\alpha}$ ,  $F_{\phi,\alpha}$ ,  $G_{z,\alpha}$ , and  $G_{\phi,\alpha}$  to be continuous across the core-cladding interface, result in four

linear equations from which  $C_\alpha^+$ ,  $C_\alpha^-$ ,  $D_\alpha^+$ , and  $D_\alpha^-$  are given in terms of  $A_\alpha$  and  $B_\alpha$ . For each set of indices  $\beta$ ,  $q$ , and  $m$ , the polarization index  $p$  labels two linearly independent choices of  $A_\alpha$  and  $B_\alpha$ . A calculation of the relations between the coefficients  $A_\alpha$ ,  $B_\alpha$ ,  $C_\alpha^+$ ,  $C_\alpha^-$ ,  $D_\alpha^+$ , and  $D_\alpha^-$ , and a construction of a biorthogonal set of radiation modes, is given in Appendix A.

We define the adjoint solution  $\tilde{\mathbf{E}}_\alpha$  to be  $\tilde{\mathbf{E}}_\alpha = (\mathbf{E}_\alpha^-)^*$ ,

where  $\tilde{\alpha} = \{-m, p, -\beta, q\}$ . It is clear that with this definition  $\tilde{\mathbf{E}}_\alpha$  is a solution to the complex conjugate of Eq. (21), such that  $\mathcal{H}^\dagger \tilde{\mathbf{g}}_\alpha = \lambda_\alpha^* \tilde{\mathbf{g}}_\alpha$  for  $\tilde{\mathbf{g}}_\alpha = \sqrt{\epsilon^*} \tilde{\mathbf{E}}_\alpha$ . The reversion of angular momentum ( $m \rightarrow -m$ ) and the direction of propagation ( $\beta \rightarrow -\beta$ ) are chosen to satisfy the biorthogonality condition (17).

The part of the generalized transverse Green's tensor related to radiation modes, may now be constructed, i.e.,

$$\mathbf{G}_{GT}^{(1)}(\mathbf{r}, \mathbf{r}'; \omega) = \sum_{m,p} \int_{\beta=-\infty}^{\infty} \int_{q=0}^{\infty} \frac{\epsilon_2 \mathbf{F}_\alpha(\rho) \mathbf{F}_{\tilde{\alpha}}(\rho') \exp[im(\phi - \phi')] \exp[i\beta(z - z')]}{N_\alpha(k_0^2 \epsilon_2 - \beta^2 - q^2)} d\beta dq, \quad (40)$$

where the normalization factor  $N_\alpha$  and the biorthogonality of radiation modes, are given by

$$\int \epsilon(\mathbf{r}) \mathbf{E}_\alpha(\mathbf{r}) \cdot \mathbf{E}_{\tilde{\alpha}'}(\mathbf{r}) d^3 r = N_\alpha \delta_{mm'} \delta_{pp'} \delta(\beta - \beta') \delta(q - q'). \quad (41)$$

Here,  $\alpha'$  is short-hand notation for  $\alpha' = \{m', p', \beta', q'\}$ .

The expression (40) is valid not only for passive fibers, but it may also be used for fibers with gain and/or absorption. The expression may be simplified by introducing two new parameters  $k$  and  $\theta$  related to  $\beta$  and  $q$  by

$$\beta = k \cos \theta, \quad (42)$$

$$q = k \sin \theta, \quad (43)$$

and by taking advantage of the identity

$$\frac{1}{x + i\epsilon} = P \frac{1}{x} - i\pi \delta(x), \quad (44)$$

where  $P$  refers to the principal value. The corresponding retarded Green's tensor, taken at  $\mathbf{r} = \mathbf{r}'$ , may then be written

$$\begin{aligned} \mathbf{G}_{GT}^{(1)}(\mathbf{r}, \mathbf{r}; \omega + i\epsilon) &= \sum_{m,p} P \left( \int_{k=0}^{\infty} \int_{\theta=0}^{\pi} \frac{\epsilon_2 \mathbf{F}_\alpha(\rho) \mathbf{F}_{\tilde{\alpha}}(\rho)}{N_\alpha(k_0^2 \epsilon_2 - k^2)} k dk d\theta \right) \\ &\quad - i \int_{\theta=0}^{\pi} I(\theta) \sin \theta d\theta, \end{aligned} \quad (45)$$

where

$$I(\theta) = \frac{\pi}{2} \sum_{m,p} \left( \frac{\epsilon_2 \mathbf{F}_\alpha(\rho) \mathbf{F}_{\tilde{\alpha}}(\rho)}{N_\alpha \sin \theta} \right)_{k=k_0 \sqrt{\epsilon_2}}. \quad (46)$$

For a fiber with absorption or gain in the core region (but not for a passive fiber) the principal value integral taken at  $\mathbf{r} = \mathbf{r}'$  does converge, and this is true for both the imaginary part and real part of the integral. The modeling of spontaneous emission in active fibers requires a calculation of the

imaginary part of the principal-value integral. However, for passive structures the calculation is greatly simplified, since in this case  $\epsilon_2 \mathbf{F}_\alpha(\rho) \mathbf{F}_{\tilde{\alpha}}(\rho) / N_\alpha$  is real, and the principal-value integral does not contribute to  $\text{Im}[\mathbf{G}_{GT}^{(1)}(\mathbf{r}, \mathbf{r}; \omega + i\epsilon)]$ , which is the term appearing in expression (12). In the second term of Eq. (45) the angle  $\theta$  may be interpreted as the off-axis angle of propagation for light emitted into radiation modes, and accordingly the expression has the form of an integration over an off-axis angular radiation pattern, where the radiation pattern  $I(\theta)$  is given by Eq. (46). This interpretation is, however, only valid for passive structures, since  $I(\theta)$  may become negative for certain angles for active structures. A similar simple calculation of radiation patterns is not possible via Eq. (45) for active structures. In this case a calculation of physically meaningful radiation patterns must take into account amplification and absorption, which is possible by calculating radiation patterns using the Poynting vector. Radiation patterns for active structures are considered in Sec. VI.

The expressions (34), (35), (36), and (37) are also valid for guided modes, where  $q$  is now a complex parameter with a positive imaginary part leading to exponential decay in  $\rho$  of the amplitude of the eigenfunction. In this case the eigenfunctions are restricted to propagation only along the  $z$  axis, and the degrees of freedom have been reduced relative to radiation modes. Therefore,  $\beta$  and  $q$  can no longer be chosen independently of one another, and only three quantization indices  $\alpha = \{m, n, \beta\}$  must be summed over. We follow the usual convention and replace  $q$  by the variable  $\gamma = -iq$ . The  $z$  component of a guided mode may then be written as

$$F_{z,\alpha}(\rho) = \begin{cases} A_\alpha J_m(\kappa\rho), & \rho \leq a, \\ C_\alpha K_m(\gamma\rho), & \rho > a, \end{cases} \quad (47)$$

$$G_{z,\alpha}(\rho) = \begin{cases} B_\alpha J_m(\kappa\rho), & \rho \leq a, \\ D_\alpha K_m(\gamma\rho), & \rho > a. \end{cases} \quad (48)$$

Here  $K_m$  is the modified Bessel function of the second kind of order  $m$ . As is also the case for radiation modes, the coefficients  $A_\alpha$ ,  $B_\alpha$ ,  $C_\alpha$ , and  $D_\alpha$  must be chosen so that the

boundary conditions are satisfied. Due to these conditions, the allowed values for  $\gamma$  become functions of  $\alpha$ , i.e.,  $\gamma = \gamma_\alpha$ . Furthermore, each mode  $m, n$  only exists for  $|\beta| \geq \beta_{m,n,c}$ , where  $\beta_{m,n,c}$  is a cutoff propagation constant such that  $\text{Re}(\gamma_\alpha) \geq 0$  for  $|\beta| \geq \beta_{m,n,c}$ . Here, we choose to use real propagation constants  $\beta$ , and accordingly the eigenvalues  $\lambda_\alpha$  become complex. We will not go into a detailed derivation of the guided modes of the fiber here, as this is a topic that has been studied extensively in the literature (see, for example Refs. [63,64]). The contribution to the Green's tensor from the guided modes may be written

$$\mathbf{G}_{GT}^{(2)}(\mathbf{r}, \mathbf{r}'; \omega) = \sum_{m,n} \int_{|\beta| \geq \beta_{m,n,c}} \frac{\varepsilon_2 \mathbf{F}_\alpha(\rho) \mathbf{F}_{\tilde{\alpha}}(\rho') e^{i\beta(z-z')} e^{im(\phi-\phi')}}{N_\alpha (k_0^2 \varepsilon_2 + \gamma_\alpha^2 - \beta^2)} d\beta, \quad (49)$$

where  $\tilde{\alpha} = \{-m, n, -\beta\}$ . The normalization factor  $N_\alpha$  and biorthogonality relation for guided modes are given by

$$N_\alpha \delta_{mm'} \delta_{nn'} \delta(\beta - \beta') = \int \varepsilon(\mathbf{r}) \mathbf{E}_\alpha(\mathbf{r}) \cdot \mathbf{E}_{\tilde{\alpha}'}(\mathbf{r}) d^3r. \quad (50)$$

As was also the case for radiation modes, the imaginary part may be greatly simplified for passive structures by taking advantage of the identity (44), i.e.,

$$\begin{aligned} \text{Im}(\mathbf{G}_{GT}^{(2)}(\mathbf{r}, \mathbf{r}; \omega + i\epsilon)) \\ = -\pi \sum'_{m,n} \left( \frac{\varepsilon_2 \mathbf{F}_\alpha(\rho) \mathbf{F}_{\tilde{\alpha}}(\rho)}{N_\alpha \left| \frac{d}{d\beta} (\beta^2 - \gamma_\alpha^2) \right|} \right)_{\beta^2 - \gamma_\alpha^2 = k_0^2 \varepsilon_2}. \end{aligned} \quad (51)$$

Here, the prime means that only modes  $m, n$  with  $|\beta_{m,n,c}| < k_0 \sqrt{\varepsilon_2}$  should be summed over.

The generalized transverse part of the retarded Green's tensor may now be obtained as the sum of the two contributions given in Eqs. (40) and (49). The double-transverse Green's tensor may be obtained by replacing the generalized transverse fields in the numerators of Eqs. (40) and (49) by the transverse part of these fields. A method for calculating the transverse part of the generalized transverse fields is given in Appendix B. For fibers with relatively weak index contrast, the difference between the generalized transverse and the usual transverse [26,61] Green's tensor is almost negligible. However, this may not be the case for dielectric structures with high index contrasts such as those investigated by, for example, Dodabalapur *et al.* [65].

## V. SPONTANEOUS EMISSION IN A PASSIVE FIBER

In this section we will evaluate the spontaneous emission going into radiation modes and bound modes for a passive optical fiber. Only for passive fibers is it really meaningful to consider the fraction of spontaneous emission going into spe-

cific modes, in this case, due to the existence of a complete set of orthogonal eigenmodes. In the following section we will then consider physically meaningful radiation patterns for active fibers, taking into account the effect of gain and absorption.

The passive fiber under concern, is defined by a core refractive index  $n_1 = 1.45$ , a cladding refractive index  $n_2 = 1.43$ , and a core radius  $a = 2 \mu\text{m}$ . The emitter is located at  $\mathbf{r}_0 = (\rho_0, \phi_0, z_0)$  in the fiber. In order to properly normalize the spontaneous emission, we will introduce the spontaneous emission  $\Gamma_{hom}$  from an emitter in a passive homogeneous dielectric material with the same refractive index as the core of the optical fiber, i.e.,

$$\Gamma_{hom} = \frac{\omega_0^3 \mu^2 n_1}{\hbar \varepsilon_0 c^3 3\pi}, \quad (52)$$

where  $\mu$  is the norm of the dipole vector  $\boldsymbol{\mu}$ . This expression is easily obtained using Eq. (12) for the case of a dipole at position  $\rho_0 = 0$ , and dipole orientation along the  $z$  axis, or by using the results for homogeneous dielectrics given in Ref. [32].

An example of the position dependence of the spontaneous emission for an emitter with transition wavelength 1560 nm in the core of the fiber, is shown in Fig. 2 for the case of dipole orientation along the  $z$  axis ( $\Gamma_z$ ) and for the average over the two in-plane dipole orientations  $x$  and  $y$ , i.e.,  $\Gamma_\perp = (\Gamma_x + \Gamma_y)/2$ . The spontaneous emission averaged over all dipole orientations is given by  $\Gamma = (\Gamma_x + \Gamma_y + \Gamma_z)/3$ . The spontaneous emission into radiation modes clearly shows a modulation with position in the fiber, which may be explained as a cavity effect. The periodicity  $\Delta\rho_0$  in the spontaneous emission with position in the fiber core due to constructive destructive interference arising from reflections at the core-cladding interface, should be roughly equal to one-half wavelength in the medium, i.e.,

$$\frac{\Delta\rho_0}{a} \approx \frac{\lambda_0}{2an_1}. \quad (53)$$

From this expression, we obtain the periodicity  $\Delta\rho_0/a \approx 0.27$ . From the total emission for emitters with  $z$  dipole direction [see Fig. 2(c)] the distance between local maxima or local minima is in the range from 0.26 to 0.28.

Almost no spontaneous emission goes into guided modes for the case of dipole orientation along the  $z$  axis. This is due to the electric field of the fundamental guided mode of the optical fiber having a negligible field component along the  $z$  axis, i.e., the electric field is primarily in the  $xy$  plane. Emission into radiation modes for dipole orientation in the  $xy$  plane is clearly lower compared to the case of dipole orientation along the  $z$  axis. This is due to part of the spontaneous emission being captured by the optical waveguide. From the total spontaneous emission into both guided modes and radiation modes, we see that the total spontaneous emission is close to  $\Gamma_{hom}$  for all positions. Therefore Fig. 2(b) also gives a good estimate for the spontaneous emission factor, i.e., the fraction of the spontaneous emission going into the guided modes of the optical waveguide. The decrease in the total

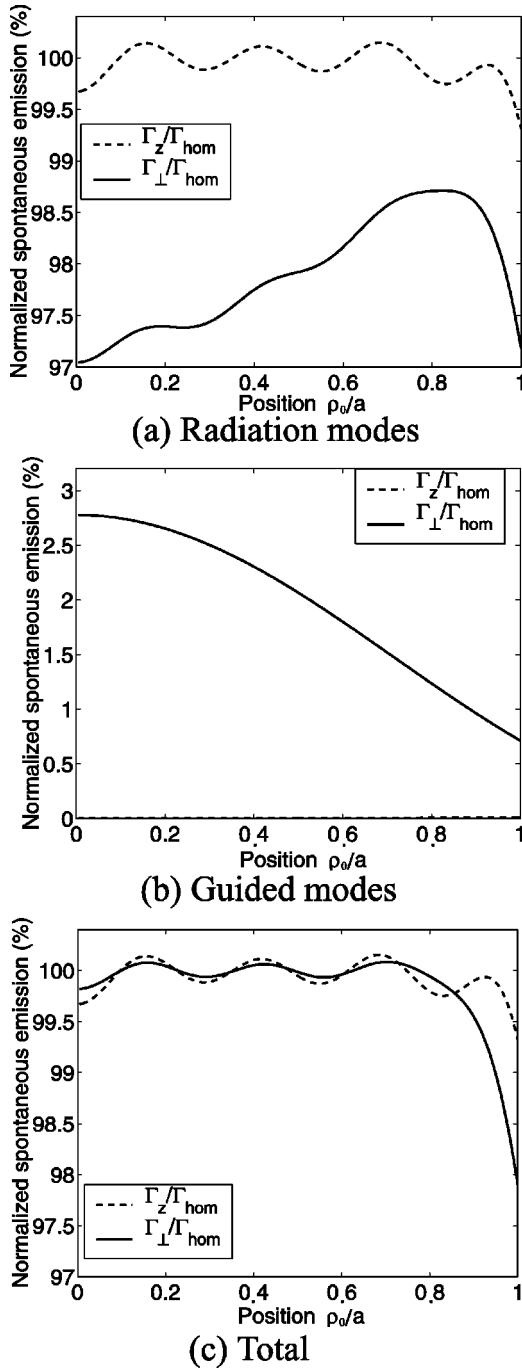


FIG. 2. Spontaneous emission as a function of position for an emitter in the core of a step-index fiber with core refractive index  $n_1=1.45$ , cladding refractive index  $n_2=1.43$ , and core radius  $a=2\ \mu\text{m}$ . The emission wavelength is  $\lambda_0=1560\ \text{nm}$ .

spontaneous emission near the core-cladding interface, may be explained from the fact that the spontaneous emission in homogeneous dielectrics scales with the refractive index [see Eq. (52)], and emitters close to the core-cladding interface are affected by the presence of a material with a lower refractive index. The total emission near the core-cladding interface is clearly different for the different dipole orientations. This may be explained from the fact that the boundary conditions at the core-cladding interface depend on the field

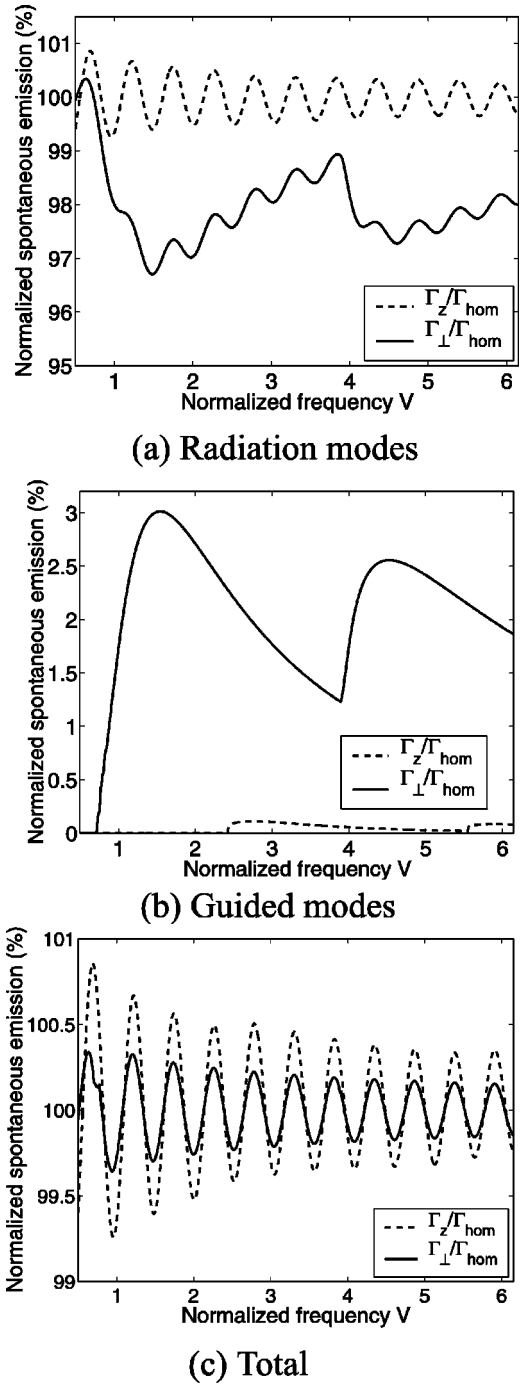


FIG. 3. Spontaneous emission as a function of normalized frequency for an emitter located in the center of the core of a step-index fiber with  $n_1=1.45$ ,  $n_2=1.43$ ,  $a=2\ \mu\text{m}$ .

orientation, i.e., the tangential electric-field components are constant across the interface, whereas normal components differ by the factor  $n_1^2/n_2^2=1.03$ .

Figure 3 shows the spontaneous emission as a function of normalized frequency  $V=k_0a\sqrt{n_1^2-n_2^2}$  for an emitter in the center of the fiber core ( $\rho_0=0$ ). Also, in this case, the periodic oscillations, seen in the spontaneous emission, is due to constructive destructive interference arising due to reflections at the core-cladding interface. The oscillations in the

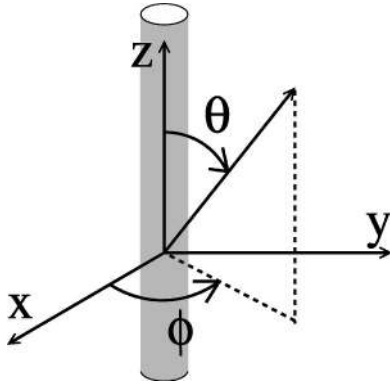


FIG. 4. Illustration of an optical fiber oriented along the  $z$  axis in a Cartesian coordinate system  $(x, y, z)$ . Two angles  $\theta$  and  $\phi$  are introduced.

total spontaneous emission [Fig. 3(c)] are clearly larger for emitters oriented along the  $z$  axis. Emitters with this orientation emit primarily in the  $xy$  plane, and interference effects due to reflections from the core-cladding interface are therefore more pronounced. Emitters placed in the center of the waveguide with dipole orientation in the  $xy$  plane are only allowed to interact with modes having angular momentum  $m = \pm 1$ . The fundamental fiber mode starts to become localized for normalized frequencies  $V$  just below 1. There are also guided modes with angular momentum  $\pm 1$  that become allowed for  $V \geq 4$ . Around both frequencies  $V=1$  and  $V=4$ , a strong decrease is seen in the spontaneous emission going into radiation modes for in-plane dipoles. This is compensated by a corresponding strong increase in the spontaneous emission into guided modes, and the total rate of spontaneous emission is oscillating with frequency around  $\Gamma_{hom}$ . The spontaneous emission into guided modes for emitters with dipole orientation along the  $z$  axis, starts at normalized frequencies around  $V \approx 2.4$ . This frequency corresponds to the single-mode cutoff of step-index optical fibers [62].

## VI. SPONTANEOUS EMISSION ANGULAR RADIATION PATTERNS

The emission of radiation from active dielectric microstructures, will in general differ from the spontaneous emission due to the amplification or absorption of light. In this section we will present radiation patterns for active optical fibers, taking into account the effect of the active material using a Poynting-vector approach.

In Fig. 4 the optical fiber is oriented along the  $z$  axis in a Cartesian coordinate system  $(x, y, z)$ . Two angles  $\theta$  and  $\phi$  are introduced. The angular radiation pattern is defined as the radial emission per unit solid angle as a function of the direction given by  $\theta$  and  $\phi$ . In evaluating the angular spontaneous emission pattern in a rigorous way, we may note that, far away from the active fiber, the power flux is radial, and the power flux  $dP$  per unit solid angle  $d\Omega$  may be written in the form

$$\frac{dP}{d\Omega} = R^2 |\mathbf{S}(\mathbf{R})|, \quad (54)$$

where  $\mathbf{R}$  is the position relative to the source,  $R = |\mathbf{R}|$ , and  $\mathbf{S}$  is the Poynting vector, which for large distances  $R$  reduces to

$$\mathbf{S} = 2 \frac{\mathbf{R}}{R} \varepsilon_0 n_2 c \langle \hat{\mathbf{E}}^\dagger \cdot \hat{\mathbf{E}} \rangle. \quad (55)$$

The emission rate into radiation modes per unit solid angle  $d\Omega$  is given by

$$\frac{d\Gamma}{d\Omega} = \lim_{R \rightarrow \infty} \frac{1}{\hbar \omega} |\mathbf{S}(\mathbf{R})| R^2. \quad (56)$$

Note that this expression only equals the *spontaneous* emission for passive structures, since for the case of amplifying or absorbing structures, the spontaneously emitted light has been amplified or attenuated by the active medium.

The electric field at large distances is given in terms of the Green's tensor and generating currents by

$$\hat{\mathbf{E}}(\mathbf{R}) = \int \int \mathbf{G}(\mathbf{R}, \mathbf{r}'; \omega + i\epsilon) \cdot [-i\mu_0 \omega \hat{\mathbf{j}}_T(\mathbf{r}')] d^3 r'. \quad (57)$$

According to this equation, and the properties of the Green's tensor, the transverse currents generate a generalized transverse electric field. However, only the transverse component of these fields contribute to the rate of spontaneous emission. At large distances from the fiber, the longitudinal component of the electric field is negligible, and the field at such a distance is transverse.

For the case of delta-correlated currents, the amplitude of the electric field squared at position  $\mathbf{R}$  generated by the transverse part of a dipole current at position  $\mathbf{r}_0$  with dipole orientation  $\mathbf{e}_i$ , is given by

$$\begin{aligned} & \langle \hat{\mathbf{E}}(\mathbf{R})^\dagger \cdot \hat{\mathbf{E}}(\mathbf{R}) \rangle \\ &= \mu_0^2 \omega^4 \mu^2 \left| \int \mathbf{G}(\mathbf{R}, \mathbf{r}'; \omega) \cdot \delta_T(\mathbf{r}', \mathbf{r}_0) \cdot \mathbf{e}_i d^3 r' \right|^2, \end{aligned} \quad (58)$$

and the spontaneous emission per unit solid angle in the direction given by  $\mathbf{R}$ , may in the limit of large distances  $R = |\mathbf{R}|$  be written

$$\frac{d\Gamma}{d\Omega} = \frac{\omega^3 \mu^2 \sqrt{\varepsilon_2}}{\hbar \varepsilon_0 c^3} 2 \lim_{R \rightarrow \infty} \left| \int \mathbf{G}(\mathbf{R}, \mathbf{r}'; \omega) \cdot \delta_T(\mathbf{r}', \mathbf{r}_0) \cdot \mathbf{e}_i d^3 r' \right|^2. \quad (59)$$

For a gain medium, the expression (59) only gives the amplified emission from the dipole at  $\mathbf{r}_0$ . We ignore the amplified spontaneous emission from the gain medium itself. The latter can be included by calculating  $\langle \hat{\mathbf{E}}^\dagger \cdot \hat{\mathbf{E}} \rangle$ , using Eq. (57) and the correlation relation (8).

For large  $R$ , the electromagnetic field behaves as a plane wave with the wave number  $k_0 \sqrt{\varepsilon_2} = \sqrt{\beta^2 + q^2}$ , and the magnitude of  $\beta$  and  $q$  is determined from the off-axis angle  $\theta$  of the vector  $\mathbf{R}$ , i.e.,  $\beta = k_0 \sqrt{\varepsilon_2} \cos \theta$  and  $q = k_0 \sqrt{\varepsilon_2} \sin \theta$ . With this restriction imposed on  $\beta$ ,  $q$ , and using the notation for

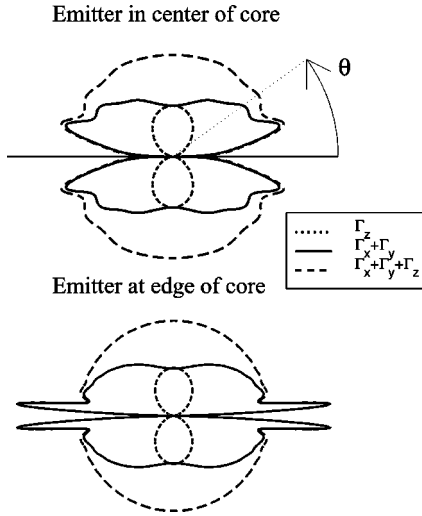


FIG. 5. Spontaneous emission as a function of the off-axis angle for an emitter in the center of the core and an emitter at the edge of the core of a step-index fiber with  $n_1=1.45$ ,  $n_2=1.43$ ,  $a=2 \mu\text{m}$ , and for  $\lambda_0=1560 \text{ nm}$ .

radiation modes in Sec. IV, a general expression for the angular emission pattern for active fibers generated by currents at position  $(\rho_0, \phi_0, z_0)$  is given by

$$\frac{d\Gamma}{d\Omega} = \frac{\omega^3 \mu^2 \sqrt{\epsilon_2}}{\hbar \epsilon_0 c^3} 2 \frac{(2\pi)^2}{k_0^2 \epsilon_2 \sin^4 \theta} \times \left( \left| \sum_{m,p} C_{\alpha}^+ e^{-i(m\pi/2)} \frac{F_{i,\tilde{\alpha}}^{-T}(\rho_0) e^{im(\phi-\phi_0)}}{N_{\alpha}} \right|^2 + \left| \sum_{m,p} \sqrt{\frac{\mu_0}{\epsilon_0 \epsilon_2}} D_{\alpha}^+ e^{-i(m\pi/2)} \frac{F_{i,\tilde{\alpha}}^{-T}(\rho_0) e^{im(\phi-\phi_0)}}{N_{\alpha}} \right|^2 \right). \quad (60)$$

Here,  $F_{i,\tilde{\alpha}}^{-T}(\rho_0) e^{-im\phi_0} e^{-i\beta z_0}$  is the component of the field  $\mathbf{E}_{\alpha}^{-T}(\mathbf{r}_0)$  in the direction  $\mathbf{e}_i$ , corresponding to the orientation of the dipole vector. Note that the emission per unit solid angle Eq. (60) depends on both angles  $\theta$  and  $\phi$ , whereas the radiation pattern Eq. (46) does not depend on  $\phi$ .

Figure 5 shows a calculation of the off-axis angular spontaneous emission pattern Eq. (60) averaged over the angle  $\phi$  for an emitter in the center of the fiber core and at the edge of the fiber core, respectively, for a passive step-index fiber with core refractive index 1.45, cladding refractive index 1.43, and core radius  $2 \mu\text{m}$ . The results presented in this figure may also be obtained directly using the off-axis angular radiation pattern given in Eq. (46). In fact, for a passive fiber, the sum of expression (60) integrated over all solid angles and the corresponding contribution from guided modes, will equal the expression (12). The transition wavelength of the emitter is 1560 nm. The radiation pattern for emitters oriented along the  $z$  axis ( $\Gamma_z$ ) closely resembles a figure eight ( $\Gamma_z \propto \sin^2 \theta$ ), which is the radiation pattern generated by a dipole in a homogeneous dielectric medium. Part of the radiation generated by emitters oriented in the  $xy$  plane, is captured by the optical waveguide, and for small

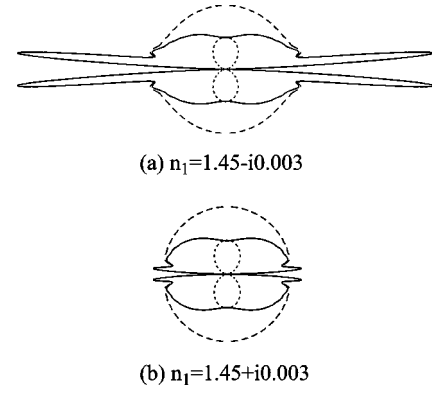


FIG. 6. Spontaneous emission as a function of the off-axis angle for an emitter at the edge of the core of a step-index fiber with  $a=2 \mu\text{m}$ ,  $n_2=1.43$  and (a)  $n_1=1.45-i0.003$ , (b)  $n_1=1.45+i0.003$ , and for  $\lambda_0=1560 \text{ nm}$ .

off-axis angles  $\theta$ , the radiation pattern is clearly modified relative to the case of a homogeneous dielectric medium ( $\Gamma_x + \Gamma_y \propto 1 + \cos^2 \theta$ ). The radiation patterns, shown in Fig. 5, are characterized by a peak for a small off-axis angle  $\theta$ . As the transition wavelength decreases and approaches the cut-off wavelength for the next guided mode, the peaks will grow larger and the peak angle will move toward 0. As the wavelength drops below the cutoff wavelength, the peaks being nearly parallel to the  $z$  axis will disappear, and a new guided mode will appear. This explains that although abrupt changes with frequency is possible for the emission into radiation modes and guided modes, a similar abrupt change should not be expected in the sum of emission into radiation modes and guided modes. This is also in agreement with the results shown in Fig. 3.

Figure 6 shows a similar calculation of the angular emission patterns averaged over the angle  $\phi$  for the case of emitters at the edge of the fiber core for the cases of fibers with amplification and absorption. Clearly, by comparing Figs. 5 and 6, the effect from absorption in the fiber is a reduction in the peaks seen for small angles in Fig. 5(b), and the effect of gain is that these peaks are enhanced. The effect of an active medium will be most pronounced for small off-axis angles  $\theta$ , where the emitted light will interact with the active material for a longer time and over longer lengths. Consequently, the amplification of spontaneous emission from in-plane emitters ( $\Gamma_x + \Gamma_y$ ) will be more efficient compared to the case of emitters directed along the  $z$  axis ( $\Gamma_z$ ). The spontaneous emission, as a function of position into radiation modes for a passive structure, was given in Fig. 2(a). In this case, the emission for in-plane emitters [ $\Gamma_{\perp} = (\Gamma_x + \Gamma_y)/2$ ] is clearly lower for all positions  $\rho_0 \leq a$  compared to the case of  $z$ -directed emitters ( $\Gamma_z$ ). As was the case for Fig. 5, the Fig. 2(a) may also be obtained by integrating Eq. (60) over all solid angles. The physically measurable emission into radiation modes must reflect the effect of amplification or absorption for structures with an active medium. Figure 7 shows the measurable emission into radiation modes as a function of position  $\rho_0$  for a fiber with gain. The emission for both the considered orientations of the currents has increased relative to the spontaneous emission in the corresponding passive

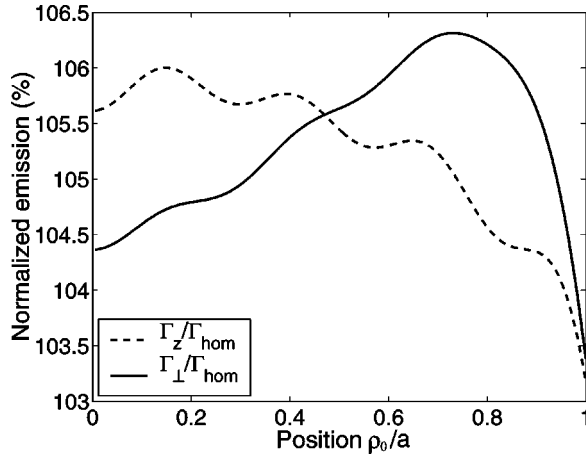


FIG. 7. Emission into radiation modes as a function of position for an active fiber with  $n_1=1.45-i0.003$  (gain),  $n_2=1.43$ ,  $a=2 \mu\text{m}$ , and for  $\lambda_0=1560 \text{ nm}$ .

fiber, and the emission from in-plane oriented emitters ( $\Gamma_{\perp}$ ) has been amplified more, relative to the case of  $z$ -directed emitters ( $\Gamma_z$ ). For both orientations of the emitter, the amplification is clearly larger for emitters in the center of the core ( $\rho_0=0$ ) relative to emitters at the edge of the core ( $\rho_0=a$ ).

For active fibers, where the distribution of active material is a function of the radius  $\rho$  only, averaging over the angle  $\phi$  is reasonable. However, the Poynting-vector approach does allow the dependence on the angle  $\phi$ , relative to the angle  $\phi_0$ , related to the position of the emitter, to be taken into account in the radiation patterns. An example is given for  $\phi-\phi_0=0, \pi$  in Fig. 8 for a fiber with absorption, a passive fiber, and a fiber with gain. The emitter is placed at the edge of the core. The radiation patterns are clearly asymmetric due to the asymmetric position of the emitter ( $\rho_0 \neq 0$ ). The effect of amplification or absorption is strongest for  $\phi-\phi_0=\pi$ , since this direction corresponds to the opposite side of the active fiber relative to the emitter. Also, in this case, the peaks observed for small off-axis angles  $\theta$  for a passive fiber, increases (decreases) for a fiber with gain (absorption).

## VII. CONCLUSION

In conclusion, a general method has been developed for the modeling of spontaneous emission in active dielectric

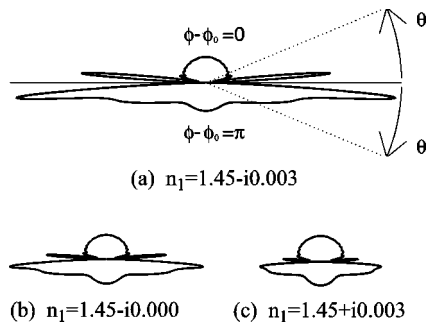


FIG. 8. Spontaneous emission as a function of the off-axis angle for an emitter at the edge of the core of a step-index fiber with  $a=2 \mu\text{m}$ ,  $n_2=1.43$ , (a)  $n_1=1.45-i0.003$ , (b)  $n_1=1.45+i0.000$ , (c)  $n_1=1.45+i0.003$ , and for  $\lambda_0=1560 \text{ nm}$ .

microstructures. The fully vectorial method is based on the classical retarded electric-field Green's tensor, giving the relation between the quantum-mechanical operators for the electric field and the generating currents. Taking advantage of the currents related to spontaneous radiative decay being transverse currents, allows a formalism, where only the double-transverse Green's tensor needs to be calculated. The double-transverse part of the Green's tensor thus becomes a key ingredient in the model for spontaneous emission. A general approach was given for the construction of the Green's tensor for active dielectric microstructures. This approach does not rely on the existence of a complete power orthogonal set of electromagnetic modes, and is therefore valid for dielectric structures with absorption and/or amplification.

The method for spontaneous emission was applied to a fiber amplifier, and as a first step the Green's tensor for this structure was calculated. One of the terms in the calculated expression for the electric-field Green's tensor was interpreted as an integration over an off-axis angular radiation pattern, and agreement has been found with this interpretation and the radiation patterns calculated using the Poynting vector. A similar interpretation of the expression for the Green's tensor for fibers with gain or absorption is not possible, since a physically measurable radiation pattern must take into account the amplification or absorption of spontaneously emitted light due to the presence of an active medium. A Poynting-vector approach has the advantage that radiation patterns that depend on both the off-axis angle and the azimuthal angle, may be obtained.

For a passive fiber, the expressions for the relevant parts of the Green's tensor become particularly simple, and for passive fibers the spontaneous emission going into radiation modes and guided modes was studied. Although the emission into these two types of modes is clearly different, and also depend on the orientation of the generating currents, the sum of these two contributions oscillates closely around the rate of spontaneous emission for a homogeneous dielectric medium with the same refractive index as the fiber core. The oscillations observed with position and frequency are explained as a consequence of destructive and constructive interference due to reflections from the interface between the fiber core and cladding. Abrupt changes with frequency in the emission into radiation modes and guided modes were observed at frequencies where new guided modes appear. Similar abrupt changes with frequency are not observed in the sum of these two contributions. This was explained from radiation patterns calculated using the Poynting-vector approach, where strong peaks, being nearly parallel to fiber axis, exist just before the next guided mode appears. The peaks disappear as the new guided mode appears.

The effect of an active medium on the radiation pattern is strongest for emission propagating at small off-axis angles. In particular, the peaks transforming into a new guided mode as the frequency increases, are enhanced (attenuated) for a core region with gain (absorption).

## APPENDIX A: BIORTHOGONALITY AND NORMALIZATION OF RADIATION MODES

This appendix concerns the relations between the coefficients  $A_{\alpha}$ ,  $B_{\alpha}$ ,  $C_{\alpha}^{+}$ ,  $C_{\alpha}^{-}$ ,  $D_{\alpha}^{+}$ , and  $D_{\alpha}^{-}$  in Eqs. (38) and (39)

for a given set of quantization parameters  $m, \beta$ , and  $q$ , and we will use the notation introduced in Sec. IV. Due to the boundary conditions at the core-cladding interface, these coefficients are not independent. Furthermore, in this appendix, a biorthogonal set of radiation modes is constructed, and a normalization integral for the modes is calculated.

The relations between  $C_\alpha^+$ ,  $C_\alpha^-$ ,  $D_\alpha^+$ ,  $D_\alpha^-$ , and  $A_\alpha$  and  $B_\alpha$  may be expressed by first introducing a number of constants

$$T = H_m^{(1)'}(qa)H_m^{(2)}(qa) - H_m^{(2)'}(qa)H_m^{(1)}(qa) = \frac{4i}{\pi qa}, \quad (\text{A1})$$

$$K_1 = i \frac{\beta}{a} m J_m(\kappa a) H_m^{(2)}(qa) \sqrt{\frac{\beta^2 + q^2}{\varepsilon_2} \frac{\varepsilon_2 - \varepsilon_1}{\kappa^2 q^2}}, \quad (\text{A2})$$

$$K_2 = i \frac{\beta}{a} m J_m(\kappa a) H_m^{(1)}(qa) \sqrt{\frac{\beta^2 + q^2}{\varepsilon_2} \frac{\varepsilon_2 - \varepsilon_1}{\kappa^2 q^2}}, \quad (\text{A3})$$

$$M_1 = \frac{1}{\kappa} J_m'(\kappa a) H_m^{(2)}(qa) - \frac{1}{q} J_m(\kappa a) H_m^{(2)'}(qa), \quad (\text{A4})$$

$$M_2 = \frac{1}{\kappa} J_m'(\kappa a) H_m^{(1)}(qa) - \frac{1}{q} J_m(\kappa a) H_m^{(1)'}(qa), \quad (\text{A5})$$

$$L_1 = \frac{\varepsilon_1}{\kappa} J_m'(\kappa a) H_m^{(2)}(qa) - \frac{\varepsilon_2}{q} J_m(\kappa a) H_m^{(2)'}(qa), \quad (\text{A6})$$

$$L_2 = \frac{\varepsilon_1}{\kappa} J_m'(\kappa a) H_m^{(1)}(qa) - \frac{\varepsilon_2}{q} J_m(\kappa a) H_m^{(1)'}(qa), \quad (\text{A7})$$

where here ( $'$ ) denotes the derivative with respect to the argument.

In terms of these constants, the relations between  $A_\alpha$ ,  $B_\alpha$ ,  $C_\alpha^+$ ,  $C_\alpha^-$ ,  $D_\alpha^+$ , and  $D_\alpha^-$ , obtained from the boundary conditions, may be written

$$C_\alpha^+ = \frac{q}{T \varepsilon_2} (A_\alpha L_1 + \mu_0 c B_\alpha K_1), \quad (\text{A8})$$

$$C_\alpha^- = \frac{q}{T^* \varepsilon_2} (A_\alpha L_2 + \mu_0 c B_\alpha K_2), \quad (\text{A9})$$

$$\mu_0 c D_\alpha^+ = -\frac{q}{T} (A_\alpha K_1 - \mu_0 c B_\alpha M_1), \quad (\text{A10})$$

$$\mu_0 c D_\alpha^- = -\frac{q}{T^*} (A_\alpha K_2 - \mu_0 c B_\alpha M_2). \quad (\text{A11})$$

Clearly, only two coefficients are linearly independent, and the index  $p$  will be used to label two such linearly indepen-

dent solutions. These two solutions must be chosen so that the biorthogonality requirement

$$\int \varepsilon(\mathbf{r}) \mathbf{E}_\alpha(\mathbf{r}) \cdot \mathbf{E}_{\alpha'}^*(\mathbf{r}) d^3 r = N_\alpha \delta_{mm'} \delta_{pp'} \delta(\beta - \beta') \delta(q - q') \quad (\text{A12})$$

is satisfied. Similar to what was reported in Ref. [66] for dielectric waveguides, all finite terms resulting from the integration in the fiber core, will cancel with each other. The singular terms that give rise to the Dirac delta functions, result only as the integration limits tend to infinity. Taking advantage of the cancellation of finite terms, we need only identify the factor  $N_\alpha$  in front of the  $\delta$  functions. Thereby, the evaluation of the integral in Eq. (A12) is aided significantly by taking advantage of the following limiting forms of the Hankel functions:

$$H_m^{(1)}(q\rho) \approx \sqrt{\frac{2}{\pi q\rho}} e^{i(q\rho - m\pi/2 - \pi/4)}, \quad \rho \gg 1/q, \quad (\text{A13})$$

$$H_m^{(2)}(q\rho) \approx \sqrt{\frac{2}{\pi q\rho}} e^{-i(q\rho - m\pi/2 - \pi/4)}, \quad \rho \gg 1/q. \quad (\text{A14})$$

Straightforward calculations then lead to

$$\begin{aligned} & \int_{\rho=0}^{\infty} [\mathbf{F}_\alpha(\rho) \cdot \mathbf{F}_{\alpha'}^*(\rho)]_{\substack{\beta=\beta' \\ m=m'}} \rho d\rho \\ &= \frac{4}{qq' \sqrt{qq'}} \left\{ \left[ (qq' + \beta^2) C_\alpha^+ C_{\alpha'}^- \right. \right. \\ & \quad \left. \left. - \frac{\mu_0}{\varepsilon_0 \varepsilon_2} \sqrt{(\beta^2 + q^2)(\beta^2 + q'^2)} D_\alpha^+ D_{\alpha'}^- \right] \delta^+(q - q') \right. \\ & \quad \left. + \left[ (qq' + \beta^2) C_\alpha^- C_{\alpha'}^+ \right. \right. \\ & \quad \left. \left. - \frac{\mu_0}{\varepsilon_0 \varepsilon_2} \sqrt{(\beta^2 + q^2)(\beta^2 + q'^2)} D_\alpha^- D_{\alpha'}^+ \right] \delta^-(q - q') \right\} \\ & \quad \times (-1)^m + \text{non-singular terms}, \quad (\text{A15}) \end{aligned}$$

where

$$\delta^\pm(q - q') = \frac{1}{2\pi} \int_{\rho=0}^{\infty} e^{\pm i(q - q')\rho} d\rho. \quad (\text{A16})$$

Note that  $\delta(q - q') = \delta^+(q - q') + \delta^-(q - q')$ .

The polarization indices  $p, p'$  represent a specific choice of the sets of coefficients  $A_\alpha, B_\alpha$  and  $A_{\alpha'}, B_{\alpha'}$  for  $\alpha = \{m, p, \beta, q\}$  and  $\alpha' = \{m, p', \beta, q\}$ . A convenient choice of coefficients is  $A_\alpha = 1, A_{\alpha'} = 1, B_\alpha = i\eta$ , and  $B_{\alpha'} = -i\eta$ , since  $\eta$  can be chosen in such a way that the two polarization modes are biorthogonal. The requirement for two modes to be biorthogonal is obtained from Eq. (A15), i.e.,

$$C_{\alpha}^{+}C_{\alpha'}^{-} - \frac{\mu_0}{\varepsilon_0\varepsilon_2}D_{\alpha}^{+}D_{\alpha'}^{-} = C_{\alpha}^{-}C_{\alpha'}^{+} - \frac{\mu_0}{\varepsilon_0\varepsilon_2}D_{\alpha}^{-}D_{\alpha'}^{+} = 0. \quad (\text{A17})$$

Using Eqs. (A8)–(A11) biorthogonal modes are obtained for

$$\eta^2 = \frac{\varepsilon_0\varepsilon_2}{\mu_0} \frac{\varepsilon_2 K_1 K_2 - L_1 L_2}{\varepsilon_2 K_1 K_2 - \varepsilon_2^2 M_1 M_2}. \quad (\text{A18})$$

For a homogeneous dielectric medium with dielectric constant  $\varepsilon_2$ , the equation (A18) reduces to the well-known  $\eta = \pm \sqrt{\varepsilon_0\varepsilon_2/\mu_0}$ .

The normalization factor  $N_{\alpha}$  is obtained from Eq. (A12) and Eq. (A15), i.e.,

$$N_{\alpha} = \varepsilon_2 (2\pi)^2 4 \frac{\beta^2 + q^2}{q^3} \left[ C_{\alpha}^{+}C_{\alpha}^{-} - \frac{\mu_0}{\varepsilon_0\varepsilon_2}D_{\alpha}^{+}D_{\alpha}^{-} \right] (-1)^m. \quad (\text{A19})$$

#### APPENDIX B: THE TRANSVERSE DELTA OPERATOR $\delta_T$ FOR NONHOMOGENEOUS DIELECTRIC MEDIA

This appendix concerns the construction of the transverse delta operator  $\delta_T$  related to a dielectric constant  $\varepsilon(\mathbf{r})$ . It is defined as the operator that projects an arbitrary vector field  $\mathbf{F}(\mathbf{r})$  onto its transverse component  $\mathbf{F}_T(\mathbf{r})$ , i.e.,  $\delta_T \mathbf{F} = \mathbf{F}_T$ , where

$$\mathbf{F} = \mathbf{F}_T + \mathbf{F}_{GL} \quad (\text{B1})$$

with  $\nabla \cdot \mathbf{F}_T = 0$  and  $\nabla \times (\mathbf{F}_{GL}/\varepsilon) = \mathbf{0}$ .

By inspection one can easily verify that

$$\mathbf{F}_{GL} = \sum_n \frac{\varepsilon(\mathbf{r}) \nabla \phi_n(\mathbf{r})}{M_n} \int [\nabla \tilde{\phi}_n(\mathbf{r}')]^* \cdot \mathbf{F}(\mathbf{r}') d^3 r', \quad (\text{B2})$$

where  $\phi_n$  and  $M_n$  are given by Eq. (28) and Eq. (29). The expression obviously satisfies the condition for  $\mathbf{F}_{GL}/\varepsilon$  being longitudinal, and the completeness of the solutions to Eq. (28) ensures that  $\mathbf{F} - \mathbf{F}_{GL}$  is transverse. Hence

$$\delta_T \mathbf{F} = \mathbf{F}_T = \mathbf{F} - \mathbf{F}_{GL}, \quad (\text{B3})$$

and

$$\begin{aligned} \delta_T^{\dagger} \mathbf{F}(\mathbf{r}) &= \mathbf{F}(\mathbf{r}) - \sum_n \frac{\nabla \tilde{\phi}_n(\mathbf{r})}{M_n^*} \\ &\times \int [\varepsilon(\mathbf{r}') \nabla \phi_n(\mathbf{r}')]^* \cdot \mathbf{F}(\mathbf{r}') d^3 r'. \end{aligned} \quad (\text{B4})$$

In the case of a passive structure (real  $\varepsilon$ ) we have

$$\delta_T^{\dagger} \mathbf{E}_n = \mathbf{E}_n^T = \mathbf{E}_n, \quad (\text{B5})$$

and

$$\delta_T^{\dagger} \nabla \phi_n = \mathbf{0} \quad (\text{B6})$$

for a generalized transverse field  $\mathbf{E}_n$  and for any solution  $\phi_n$  to Eq. (28). For Eq. (32) this implies that  $\mathbf{G}_T = \mathbf{G}_{GT}$ .

- 
- [1] E. Purcell, Phys. Rev. **69**, 681 (1946).  
[2] P. Milonni and P. Knight, Opt. Commun. **9**, 119 (1973).  
[3] M. Philpott, Chem. Phys. Lett. **19**, 435 (1973).  
[4] W. Lukosz, Phys. Rev. B **22**, 3030 (1980).  
[5] H. Yokoyama and K. Ujihara, *Spontaneous Emission and Laser Oscillations in Microcavities* (CRC, New York, 1995).  
[6] P. Milonni, *The Quantum Vacuum. An Introduction to Quantum Electrodynamics* (Academic, San Diego, 1994).  
[7] J. Rarity and C. Weisbuch, *Microcavities and Photonic Bandgaps* (Kluwer, Dordrecht, 1996).  
[8] R. Chang and A. Campillo, *Optical Processes in Microcavities* (World Scientific, Singapore, 1996).  
[9] P. Goy, J.M. Raimond, M. Gross, and S. Haroche, Phys. Rev. Lett. **50**, 1903 (1983).  
[10] G. Gabrielse and H. Dehmelt, Phys. Rev. Lett. **55**, 67 (1985).  
[11] R.G. Hulet, E.S. Hilfer, and D. Kleppner, Phys. Rev. Lett. **55**, 2137 (1985).  
[12] G. Björk, S. Machida, Y. Yamamoto, and K. Igeta, Phys. Rev. A **44**, 669 (1991).  
[13] J.-M. Gérard, B. Sermage, B. Gayral, B. Legrand, E. Costard, and V. Thierry-Mieg, Phys. Rev. Lett. **81**, 1110 (1998).  
[14] D. Deppe, L. Graham, and D. Huffaker, IEEE J. Quantum Electron. **35**, 1502 (1999).  
[15] P. Skovgaard, S. Brorson, I. Balslev, and C. Larsen, in *Microcavities and Photonic Bandgaps: Physics and Applications*, edited by J. Rarity and C. Weisbuch (Kluwer, Dordrecht, 1996).  
[16] H. Zbinden, A. Müller, and N. Gisin, in *Microcavities and Photonic Bandgaps: Physics and Applications*, edited by J. Rarity and C. Weisbuch (Kluwer, Dordrecht, 1996).  
[17] A.M. Vredenberg, N.E.J. Hunt, E.F. Schubert, D.C. Jacobsen, J.M. Poate, and G.J. Zydzik, Phys. Rev. Lett. **71**, 517 (1993).  
[18] I. Abram, I. Robert, and R. Kuszelewicz, IEEE J. Quantum Electron. **34**, 71 (1998).  
[19] E. Yablonovitch, Phys. Rev. Lett. **58**, 2059 (1987).  
[20] S. John, in *Photonic Band Gap Materials*, Vol. 315 of *NATO ASI Series, Series E, Applied Sciences*, NATO Scientific Affairs Division, edited by C. Soukoulis (Kluwer, Dordrecht, 1996), pp. 563–666.  
[21] T. Søndergaard, IEEE J. Quantum Electron. **36**, 450 (2000).  
[22] K. Busch and S. John, Phys. Rev. E **58**, 3896 (1998).  
[23] J. Joannopoulos, J. Winn, and R. Meade, *Photonic Crystals: Molding the Flow of Light* (Princeton University, Princeton, NJ, 1995).  
[24] G.S. Agarwal, Phys. Rev. A **12**, 1475 (1975).  
[25] J.M. Wylie and J.E. Sipe, Phys. Rev. A **30**, 1185 (1984).  
[26] R.J. Glauber and M. Lewenstein, Phys. Rev. A **43**, 467 (1991).  
[27] T. Gruner and D.-G. Welsch, Phys. Rev. A **53**, 1818 (1996).  
[28] S. Scheel, L. Knöll, D.-G. Welsch, and S.M. Barnett, Phys. Rev. A **60**, 1590 (1999).  
[29] R. Sprik, B. Van Tiggelen, and A. Lagendijk, Europhys. Lett. **35**, 265 (1996).  
[30] H.T. Dung, L. Knöll, and D.-G. Welsch, Phys. Rev. A **57**, 3931 (1998).

- [31] B. Huttner and S.M. Barnett, Phys. Rev. A **46**, 4306 (1992).
- [32] S.M. Barnett, B. Huttner, R. Loudon, and R. Matloob, J. Phys. B **29**, 3763 (1996).
- [33] A. Tip, Phys. Rev. A **56**, 5022 (1997).
- [34] S. Scheel, L. Knöll, and D.-G. Welsch, Phys. Rev. A **58**, 700 (1998).
- [35] M.S. Yeung and T.K. Gustafson, Phys. Rev. A **54**, 5227 (1996).
- [36] W. Vogel and D.-G. Welsch, *Lectures on Quantum Optics* (Akademie-Verlag, Berlin, 1994).
- [37] H.T. Dung, L. Knöll, and D.-G. Welsch, Phys. Rev. A **62**, 053804 (2000).
- [38] K. Petermann, IEEE J. Quantum Electron. **QE-15**, 566 (1979).
- [39] H. Haus and S. Kawakami, IEEE J. Quantum Electron. **QE-21**, 63 (1985).
- [40] C. Henry, J. Lightwave Technol. **LT-4**, 288 (1986).
- [41] I. Deutsch, J. Garrison, and E. Wright, J. Opt. Soc. Am. B **8**, 1244 (1991).
- [42] B. Tromborg, H. Lassen, and H. Olesen, IEEE J. Quantum Electron. **30**, 939 (1994).
- [43] R. Marani and M. Lax, Phys. Rev. A **52**, 2376 (1995).
- [44] C. Henry and R. Kazarinov, Rev. Mod. Phys. **68**, 801 (1996).
- [45] A.E. Siegman, Phys. Rev. A **39**, 1253 (1989).
- [46] A.E. Siegman, Phys. Rev. A **39**, 1264 (1989).
- [47] W.A. Hamel and J.P. Woerdman, Phys. Rev. A **40**, 2785 (1989).
- [48] A.E. Siegman, Appl. Phys. B: Lasers Opt. **60**, 247 (1995).
- [49] P. Grangier and J.-P. Poizat, Eur. Phys. J. D. **1**, 97 (1998).
- [50] M.S. Tomaš, Phys. Rev. A **51**, 2545 (1995).
- [51] M.S. Tomaš and Z. Lenac, Phys. Rev. A **56**, 4197 (1997).
- [52] M.S. Tomaš and Z. Lenac, Phys. Rev. A **60**, 2431 (1999).
- [53] H. Rigneault, S. Robert, C. Begon, B. Jacquier, and P. Moretti, Phys. Rev. A **55**, 1497 (1997).
- [54] H.P. Urbach and G.L.J.A. Rikken, Phys. Rev. A **57**, 3913 (1998).
- [55] B. Demeulenaere, R. Baets, and D. Lenstra, Proc. SPIE **2693**, 188 (1996).
- [56] C.L.A. Hooijer, G.-x. Li, K. Allaart, and D. Lenstra, Proc. SPIE **3625**, 633 (1999).
- [57] D.Y. Chu and S.T. Ho, J. Opt. Soc. Am. B **10**, 381 (1993).
- [58] H. Nha and W. Jhe, Phys. Rev. A **56**, 2213 (1997).
- [59] W. Zakowicz and M. Janowicz, Phys. Rev. A **62**, 013820 (2000).
- [60] C.L.A. Hooijer, Ph.D-thesis, Vrije Universiteit, Amsterdam, Holland, 2001.
- [61] C. Cohen-Tannoudji, J. Dupont-Roc, and G. Grynberg, *Photons and Atoms—Introduction to Quantum Electrodynamics* (Wiley, New York, 1989).
- [62] G. Agrawal, *Fiber-Optic Communication Systems* (Wiley, New York, 1992).
- [63] H.-G. Unger, *Planar Optical Waveguides and Fibres* (Clarendon, Oxford, 1977).
- [64] W. Snyder and J. Love, *Optical Waveguide Theory* (Chapman and Hall, New York, 1983).
- [65] A. Dodabalapur, M. Berggren, R.E. Slusher, Z. Bao, A. Timko, P. Schiortino, E. Laskowski, H.E. Katz, and O. Nalamasu, IEEE J. Sel. Top. Quantum Electron. **4**, 67 (1998).
- [66] R. Sammut, J. Opt. Soc. Am. **72**, 1335 (1982).